PORT SAID ENGINEERING RESEARCH JOURNAL

Faculty of Engineering - Port Said University
Volume 28 No. 2 pp: 41 : 49

Influence of Geogrid-Axial Stiffness on Bearing Capacity of Geogrid-Reinforced Fine Sand

Essam Badrawi

Structural Engineering Department, Faculty of Engineering, Zagazig University, Zagazig, Egypt, email: e.f.b.attia@gmail.com

DOI: 10.21608/PSERJ.2024.253870.1298

Received 13-12-2024,
Revised 16-1-2024,
Accepted 18-2-2024

ABSTRACT

Geosynthetics are man-made materials used to increase the compression, and shear characteristics of soil. Geogrid-reinforced material is regarded as one of the most widely used soil reinforcements. Using finite element simulation, unreinforced and reinforced fine sand are modeled in 3-D, the load-carrying capacity is investigated for both unreinforced and geogrid-reinforced fine sand supporting a square footing with different sizes. The bearing capacity ratio (BCR) of geogrid-reinforced fine sand is influenced by the use of geogrid-layers with different axial stiffnesses (J). The influence of geogrid axial stiffness is evaluated using five investigated parameters: geogrid-layers number (N), vertical spacing (h/B), geogrid width/length (b/B), first geogrid-layer depth (u/B) and square footing size (B). The geogrid-reinforced fine sand with appropriate dimensions and proper geogrid-layers number has significantly increased the square footing bearing capacity. The load-bearing capacity of geogrid-reinforced fine sand increases with geogrid axial stiffness. For a square footing width of 2.0m, the bearing capacity ratio (BCR) is 1.45 and 2.13 when the geogrid axial stiffness increases from 250 kN/m to 500 kN/m and from 250 kN/m to 1000 kN/m, respectively. The most efficient and economical values of (u/B), (b/B), (h/B) and (N) are 0.30, 3.0, 0.15 and 3.0 for all values of geogrid axial stiffness, respectively.

Keywords: Bearing Capacity, Square Footing, Geogrid Axial Stiffness and Geogrid-reinforced Fine.

1. INTRODUCTION

Bearing capacity failure in sandy soils occurs in three forms: general-shear failure, local-shear failure, and punching-shear failure. In soils with a relative density (Dr) of more than 70%, general-shear failure happens; in soils with a relative density of between 30% and 70%, local-shear failure happens; and in sand with a relative density of less than 30%, punching-shear failure happens. Fine sand has a limited bearing capacity to support the loads of structures that having a low value of relative density (Dr). Fine sand reinforced with a geogrid-layer is a popular improvement technique for increasing soil load-bearing capacity in compression and shear [1]. The main objective of the geogrid-layer is to restrict the movement of soil particles in both lateral and vertical directions. It is also used to distribute vertical pressure over a wider area. The bearing capacity of reinforced-soil changed with various factors such as type of reinforcement materials, number of reinforcement layers (N), ratios of various parameters of reinforcement materials and footing such as footing width (B), first reinforcement-layer depth (u/B), vertical spacing between consecutive reinforcement-layers (h/B), length of layer-reinforcement (b/B), footing depth from ground level (Df/B), soil-type, soil-texture, soil unit-weight (or density), etc.. The soil bearing capacity ratio (BCR) is the ratio between the bearing capacity of reinforced and un-reinforced soil. Manisana [2] investigates the effects of footing shapes, geogrid-layers number (N) and geogrid length on soil bearing capacity, shear failure and settlement values. It was found the optimal geogrid-layers number is 4.0 and the geogrid-layers size is 4.0B x 4.0B for different footing shapes. The use of geogrid-layer increases the soil-bearing resistance and reduces settlement values due to the

change of shear failure mechanisms from local to general failure. Rowshanzamir [3] studies how geogrid-layer configuration affects the bearing capacity of sand beds with different unit weights. Three groups of geogrid-layer configurations under square footing are described as: uniform, trapezoidal, and inverse trapezoidal arrangements. The BCR values range from 1.8 to 5.35 for different geogrid-layer configurations and sand unit weights, while the maximum BCR value of geogrid-reinforced sand is obtained from inverse trapezoidal configurations. Hotti [4] describes an experimental study using square footing to illustrate the influence of first geogrid-layer depth (u/B) on the BCR values of geogrid-reinforced sand with different unit weights (16, 17, and 18 kN/m^3). The optimal value of first geogrid-layer depth (u/B) is 0.40 with a geogrid-layers number of 3.0. Budania [5] reported that the optimal depth of the first geogrid-layer (u/B) is 0.50 and the BCR value of geogrid-reinforced sand is 1.3 with a geogrid-layers number (N) of 4.0. Maruthi [5] states the more efficient (u/B) ratio of first geogrid-layer depth is 0.40 when investigating the load-carrying capacity of geogrid-reinforced sand beds with various densities of 14.45, 14.90 and 14.96 kN/m^3. Mudgal [6] presents a small-scale square footing on silty clay soil and reinforced with glasgrid and geotextile material. The maximum BCR values occur at the first reinforcement-layer depth (u/B) of 0.34 for both reinforcements. The optimal vertical spacing between reinforcements (h/B) was observed at 0.255 and 0.226 for glasgrid and geotextile, respectively. The optimal number of reinforcing layers was obtained when N = 4 and N = 3 for silty clay soil reinforced with glasgrid and geotextile, respectively. Shrigondekar [7] describes the effect of vertical spacing between geogrid-layers (h/B), the geogrid-layers number (N) and first geogrid-layer depth (u/B) on the load-carrying capacity of medium sand with a relative density (Dr) of 63.25% supporting a square footing. The maximum BCR value is 6.87 and the optimal value for both (u/B) and (h/B) ratio is 0.25. Hussam [8] investigates the influence of load eccentricity on the BCR values of geogrid-reinforced clay. The BCR values of geogrid-reinforced clay are 2.27 and 2.12 under centric and eccentric loading, respectively. The optimal values for (u/B), (h/B) and N are 0.35, 0.26 and 4.0, respectively. Das [9] studied the effect of the geogrid layer with and without prestressing on the load-bearing capacity and settlement performance. The study was carried out on three square footing sizes (0.10 m x 0.10 m, 0.20 m x 0.20 m, and 0.30 m x 0.30 m). The maximum footing size, 0.3 m x 0.3 m, gave the maximum bearing pressure, while 0.1 m x 0.1 m gave the minimum value. Furthermore, the BCR values of the footing sizes 0.10 m x 0.10 m, 0.20 m x 0.20 m, and 0.30 m x 0.30 m are 1.68, 1.53, and 1.47, respectively. Bathurst [10] investigates the effect of axial stiffness (J) on the bearing capacity of strip footing rested on clay soil with and without sand cushion, the values of axial stiffness are 300, 500, 1000, 2000 and 3000 kN/m and the BCR values are 1.61, 1.64, 1.71, 1.78 and 1.82 respectively.

A numerical analysis using Abaqus software is used to simulate unreinforced fine sand. The numerical model results of the unreinforced sand are validated with experimental results. The model was used to study the effect of geogrid axial stiffness (J) on the BCR values of square footing laid on geogrid-reinforced fine sand. the first geogrid-layer depth (u/B), vertical spacing between geogrid-layers (h/B), geogrid-layer width (b/B), geogrid-layers number (N) and square footing size (B) are also studied to determine the most efficient parameters.

2. NUMERICAL MODEL

Mechanical stabilization and soil reinforcement techniques use tensile materials like geogrid-layers, metallic strips and geotextiles. In geotechnical applications, reinforced soil technique is applied to soils with low strength values. Abaqus (Ver. 2017) [11] is utilized to simulate a 3-D model of both unreinforced and geogrid-reinforced fine sand with a relative density (D_r) of 40%. The 3-D model is symmetric about the X and Y axes, so the simulation model represents a quarter of the total model with dimensions of 20m x 20m x 20m. The effects of geogrid axial stiffness on the BCR values of geogrid-reinforced fine sand are investigated for dimensionless parameters such as (u/B), (b/B), (h/B) and (N). The fine sand is modeled by an elasto-plastic material with a non-associated flow rule and using the modified Drucker-Prager model with a hardening curve. The modified Drucker-Prager model is appropriate to soil behavior because it is capable of considering the influence of stress history, stress path, dilatancy, and the effect of the intermediate principal stress. The yield surface of the modified Drucker-Prager/cap plasticity model consists of three parts; a Drucker-Prager shear failure surface, an elliptical cap, which intersects the mean effective stress axis at a right angle, and a smooth transition region between the shear failure surface and the cap, as shown in Figure 1 [11], [12]. The modified Drucker-Prager yield surface of three different parts is described by equations (1), (2) and (3).

The Drucker-Prager shear failure surface is written as:

$$F_s = t - p\tan\beta - d = 0 \quad (1)$$

The transition surface is defined as:

$$F_t = \sqrt{(p - p_a)^2 + \left[t - \left(1 - \frac{\alpha}{\cos\beta}\right)(d + p_a\tan\beta)\right]^2} - \alpha(d + p_a\tan\beta) = 0 \quad (2)$$

The cap yield surface is written as:

$$F_c = \sqrt{(p - p_a)^2 + \left[\frac{R\,t}{1+\alpha-(\alpha/\cos\beta)}\right]^2} - R\,(d + p_a \tan\beta) = 0 \quad (3)$$

Where: (β) is the soil's angle of friction, (d) is its cohesion, (p) is the mean stress, and (q) is the Mises equivalent stress in the (p–t) plane. (R) is a material parameter (between 0.0001 and 1000.0) that controls the shape of the cap. (α) is a small number (typically 0.01–0.05) used to define a smooth transition surface between the shear failure surface and the cap. (p_a) is an evolution parameter that represents the volumetric plastic strain driven hardening/softening. The hardening/softening law is a user-defined piecewise linear function relating the hydrostatic compression yield stress, (p_b), and the corresponding volumetric inelastic (plastic and/or creep) strain. The volumetric plastic strain (ε_v) is considered as shown in equation (4).

$$p_b = f(\varepsilon_v) \quad (4)$$

The volumetric plastic strain can be expressed as described by Park and Byrne [13], equation (5).

$$\varepsilon_v = \frac{2x(1.5 - D_{ro})}{C}\sqrt{\frac{P}{P_{atm}}} \quad (5)$$

Where: ε_v = volumetric strain, %, D_{ro} = initial relative density, %, C = material constant, P = mean stress, kPa, P_{atm} = atmospheric pressure, kPa. The evolution parameter (p_a) is expressed by equation (6).

$$P_a = \frac{P_b - R\,d}{1 + R\tan\beta} \quad (6)$$

Flow stress ratio (K) defines the ratio of the yield stress in triaxial tension to the yield stress in triaxial compression. (K) is a material parameter that controls the dependence of the yield surface on the value of the intermediate principal stress, to ensure that the yield surface remains convex requires $0.778 \le k \le 1.0$. The Mohr–Coulomb parameters (c, ϕ) can be converted to Drucker–Prager parameters using equations (7) and (8) [12].

$$\tan\beta = \frac{6\,x\sin\phi}{3-\sin\phi} \quad (7)$$

$$d = \frac{18\,x\,C\,x\cos\phi}{3-\sin\phi} \quad (8)$$

Tables 1 and 2 describe fine sand the geogrid properties. The fine sand soil mass is described by an 8-node linear brick, reduced integration and hourglass control (C3D8R), while the geogrid layers are described by 4-node doubly curved general-purpose shell, finite membrane strains (S4R). To describe the full contact and interlocking between the fine sand soil and geogrid-layers, the geogrid-layer is modeled by embedded region constraints, the fine sand is defined as host region, while geogrid-layer is an embedded region with the capability to implement Abaqus/standard [11].

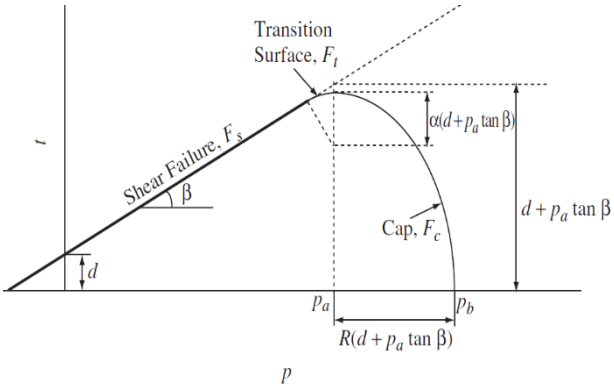

Figure 1: Yield surfaces of modified Drucker-Prager model with a hardening curve in the p–t plane [11], [12].

Table 1. Fine Sand Properties

Property	Symbol	Fine Sand
Unit weight, (kN/m^3)	γ	18.0
Poisson's ratio	υ	0.35
Young's modulus, MPa	E	20
Material Cohesion, (kPa)	c	1.6e^{-3}
	d*	0.01
Friction angle, (°)	ϕ	30.0
	β*	50.19
Cap Eccentricity	R	0.40
Init. Cap-yield surface position	––	---
Trans. surface radius	α	0.05
Flow Stress Ratio	k	1.0
Relative density	D_r	40%

Table 2. Geogrid Properties

Geogrid properties	Value
Shape of aperture	Biaxial
aperture size, mm	50 × 50 mm
Nominal rib thickness, mm	0.50, 1.0 and 2.0
Nominal rib width, mm	5.0
Axial stiffness, kN/m	250, 500, 1000
Poisson's ratio	0.35
Young's modulus, MPa	500
Unit weight, (kN/m^3)	10.0

3. NUMERICAL RESULTS

3.1. Model Validation

Abaqus 3-D software is used to simulate numerical model of unreinforced and reinforced-fine sand and verify the results of the proposed model with experimental results. The vertical pressure-settlement curve can be used to estimate the bearing capacity of unreinforced and reinforced-fine sand as shown in Figure 2, it is noted that no clear failure point was observed. If there is no clear failure pattern of the footing/soil system, the ultimate bearing capacity values are determined based on load-settlement curves using four different methods: the 10%B method, the tangent intersection method, the log-log method and

the hyperbolic method, as mentioned in [14], [15], [16]. The 10% footing width method is used in the study to estimate the ultimate bearing capacity for cases where there is no clear failure point or when the settlement value is more than 10%B. From the simulation model, the ultimate bearing capacity of unreinforced fine sand under a square footing is 165 kPa. Based on experimental results of Hotti [4] and Gupta [17], the bearing capacities of unreinforced fine sand are 162 kPa and 177 kPa, respectively. Furthermore, the bearing capacity from Meyerhof's equation is 180.46 kPa, while the ultimate bearing capacity of geogrid-reinforced fine sand when the values of u/B, b/B and N are 0.40, 3.0 and 1.0 from the Abaqus model and experimental results of Hotti [4] is 224 kPa and 226 kPa, respectively. The bearing capacity of unreinforced and geogrid-reinforced fine sand was found to be in good agreement with the experimental results.

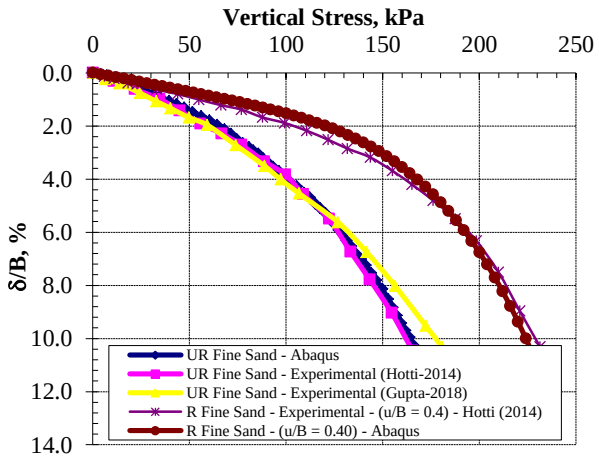

Figure 2: Settlement versus vertical stress of unreinforced and reinforced-fine sand from Abaqus and experimental results

3.2. The Bearing Capacity of Reinforced Fine Sand

The Abaqus model is considered a good tool for estimating the bearing capacity of square footing resting on reinforced fine sand. A wide range of parameters are considered in the analysis, such as first geogrid-layer depth, geogrid width, vertical spacing between the successive geogrid-layers, and the geogrid-layers number used to investigate the bearing capacity of reinforced fine sand with a geogrid-layer having different values of axial stiffness, all parameters studied are listed in Table 3.

Table 3 . Parametric study of reinforced fine sand.

Group	B, m	N	u/B	b/B	h/B	Geogrid axial stiffness, kN/m		
Sand	1.5 2 2.5	Unreinforced Fine Sand						
Group A	2	1	0.1	3	0	250	500	1000
	2	1	0.2	3	0	250	500	1000
	2	1	0.3	3	0	250	500	1000
	2	1	0.4	3	0	250	500	1000
	2	1	0.5	3	0	250	500	1000
Group B	2	1	0.3	1	0	250	500	1000
	2	1	0.3	2	0	250	500	1000
	2	1	0.3	3	0	250	500	1000
	2	1	0.3	4	0	250	500	1000
	2	1	0.3	5	0	250	500	1000
Group C	2	2	0.3	3	0.1	250	500	1000
	2	2	0.3	3	0.15	250	500	1000
	2	2	0.3	3	0.2	250	500	1000
	2	2	0.3	3	0.3	250	500	1000
	2	2	0.3	3	0.4	250	500	1000
Group D	2	1	0.3	3	0	250	500	1000
	2	2	0.3	3	0.15	250	500	1000
	2	3	0.3	3	0.15	250	500	1000
	2	4	0.3	3	0.15	250	500	1000
	2	5	0.3	3	0.15	250	500	1000
Group E	1.5	1	0.3	3	0	250	500	1000
	2.5	1	0.3	3	0	250	500	1000

3.2.1 First geogrid-layer Depth (u/B)

In the Abaqus 3-D model, the geogrid-layer is placed at different depths from the ground surface on which the vertical stress is applied to study the effect of the first geogrid-layer depth on the bearing capacity of geogrid-reinforced fine sand supporting a square footing with dimensions of 2.0 m x 2.0 m. The ratio between the first geogrid-layer depth and the footing width is described as (u/B); the (u/B) values are changed from 0.10 to 0.50 in 0.10 increments. The geogrid axial stiffness (J) is described as the relationship between the geogrid elastic modulus ($E_{geogrid}$) and geogrid thickness ($t_{geogrid}$). The geogrid axial stiffness (J) values used in the study are 250 kN/m, 500 kN/m, and 1000 kN/m. To achieve geogrid axial stiffness values, geogrid elastic modulus remains constant and is 500 MPa, while the geogrid thickness changes and is 0.50 mm, 1.0 mm, and 2.0 mm, respectively. Figure 3 shows the fine sand and geogrid-layer arrangement. Figure 4 shows the soil domain meshing, vertical displacement shading of geogrid-reinforced fine sand and vertical displacement within the geogrid-layer.

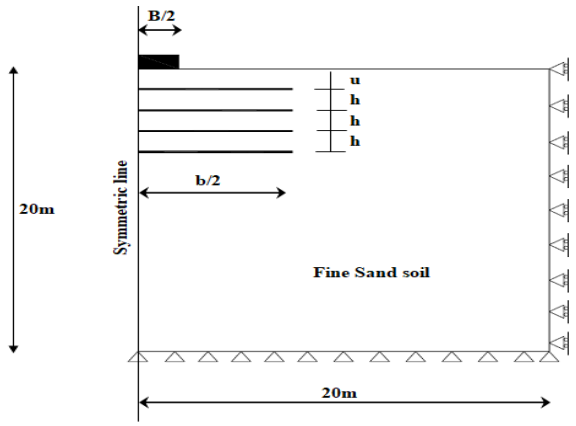

Figure 3: Fine sand and geogrid-layer arrangement

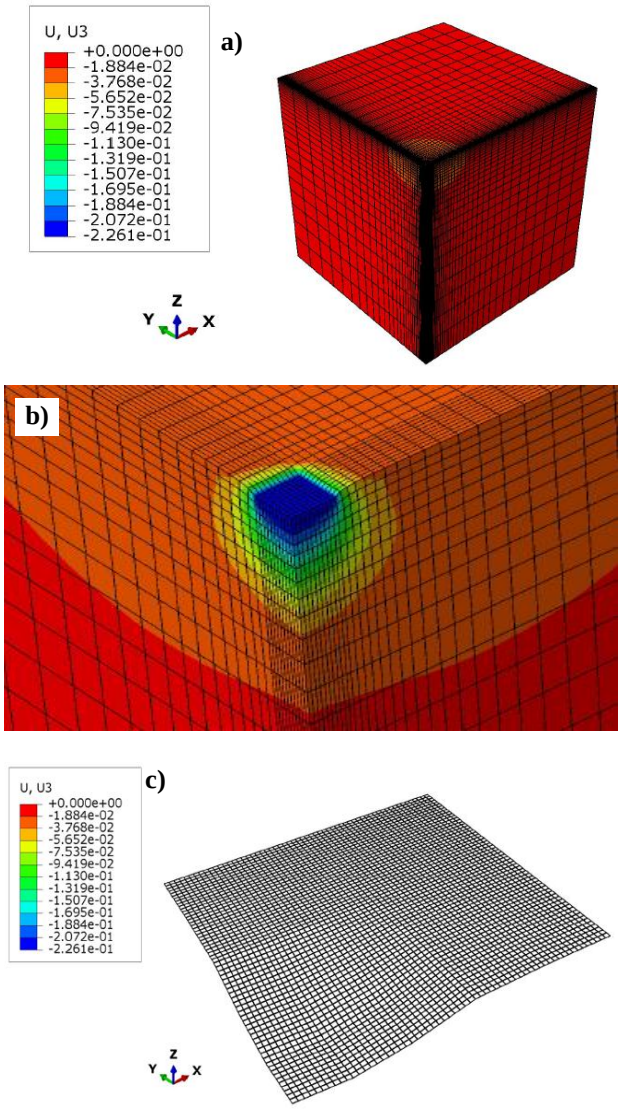

Figure 4: Numerical results of geogrid-reinforced fine sand; a) Vertical displacement of the reinforced fine sand, b) Zooming of square footing displacement and c) Vertical displacement within the geogrid-layer.

Figure 5 shows the settlement versus applied vertical stress for different cases of (u/B): a) J = 250 kN/m; b) J = 500 kN/m; c) J = 1000 kN/m; d) Bearing capacity ratio (BCR) versus (u/B) ratio and e) Bearing capacity ratio versus geogrid axial stiffness. The (BCR) values for geogrid axial stiffness (J) of 250 kN/m are 1.01, 1.44, 1.75, 1.56 and 1.25 with (u/B) values of 0.10, 0.20, 0.30, 0.40 and 0.50, respectively. The (BCR) values for geogrid axial stiffness (J) of 500 kN/m are 1.45, 2.10, 2.54, 2.25 and 1.80, while these values are 2.12, 3.07, 3.73, 3.30 and 2.61 when the geogrid axial stiffness (J) increased to 1000 kN/m at the same values of (u/B). The (BCR) values increase with the (u/B) value until (u/B) reaches 0.30 and then decrease with the increasing of (u/B); the optimal and more efficient value of (u/B) is 0.30, as shown in Figure 5-d. At (u/B) = 0.30, the increase in (BCR) value with geogrid axial stiffness (J) is 1.45 times and 2.13 times for the variation of geogrid axial stiffness from 250 kN/m to 500 kN/m and from 250 kN/m to 1000 kN/m, respectively. Figure 5-e shows the relationship between the bearing capacity ratio (BCR) and the geogrid axial stiffness. In the simulation models, the geogrid axial stiffness (J) increased to 2500 kN/m with a (u/B) value of 0.30, attempts are carried out to derive the relationship between (BCR) and (J) as described in equation (9).

$$BCR = 1.67x\ln(J) - 7.65 \qquad (u/B = 0.3) \qquad (9)$$

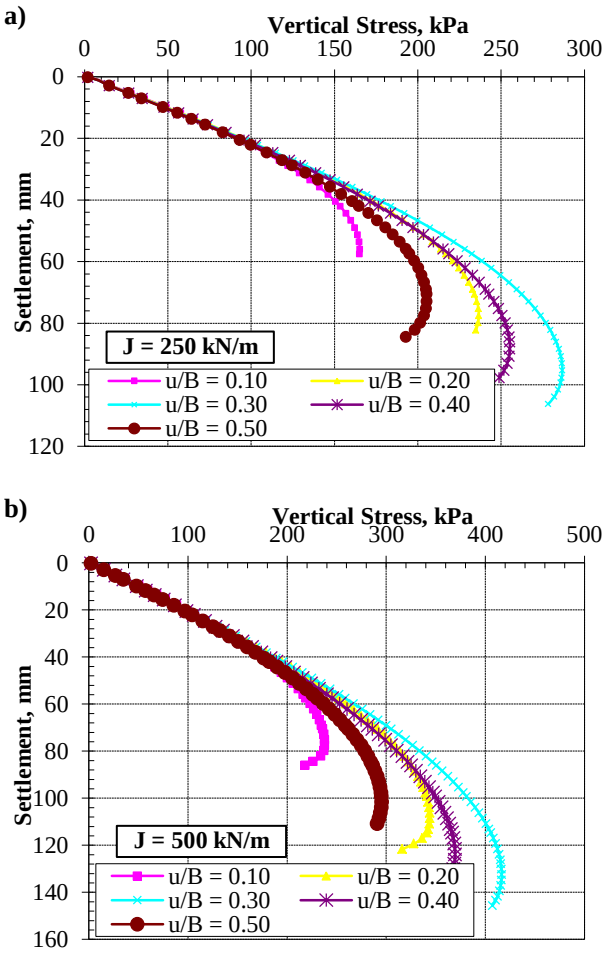

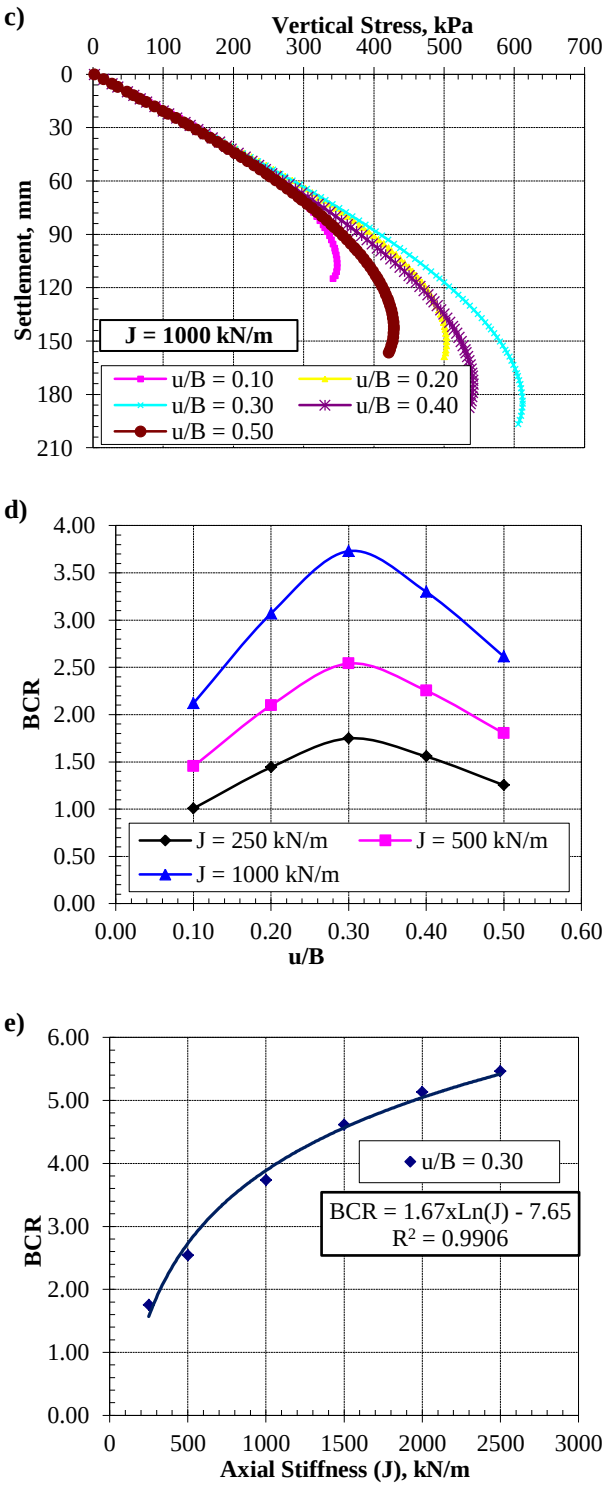

Figure 5: Settlement versus vertical stress for different values of u/B; a) J = 250 kN/m, b) J = 500 kN/m, c) J = 1000 kN/m, d) Bearing capacity ratio (BCR) versus (u/B) ratio, and e) Bearing capacity ratio versus geogrid axial stiffness

3.2.2 Geogrid-layer width (b/B)

Abaqus software is used to conduct a series of numerical models to evaluate the effect of geogrid width at the optimal value of (u/B) = 0.30. The ratio between geogrid width and the footing width (b/B) varies from 1.0 to 5.0 with an increment of 1.0 at values of geogrid axial stiffness (J) of 250 kN/m, 500 kN/m and 1000 kN/m. Figure 6 illustrates the relation between the settlement and the vertical stress under the square footing for the different values of (b/B) and geogrid axial stiffness (J). The results indicate that (BCR) values increase with the (b/B) ratio. The maximum (BCR) value occurs when the (b/B) ratio is equal to 3.0, and then the (BCR) value decreases with increasing (b/B) ratio for different cases of geogrid axial stiffness (J). At (b/B) ratio = 3.0, the (BCR) values increase with increasing geogrid axial stiffness (J), the (BCR) values are 1.75, 2.54, and 3.73 for geogrid axial stiffness of 250 kN/m, 500 kN/m, and 1000 kN/m, respectively. The results show that the increase in bearing capacity ratio (BCR) is 1.45 times and 2.13 times when the geogrid axial stiffness increases from 250 kN/m to 500 kN/m and 250 kN/m to 1000 kN/m, respectively. The bearing capacity ratio remains relatively constant once the (b/B) ratio exceeds 4.0, as shown in Figure 6-d.

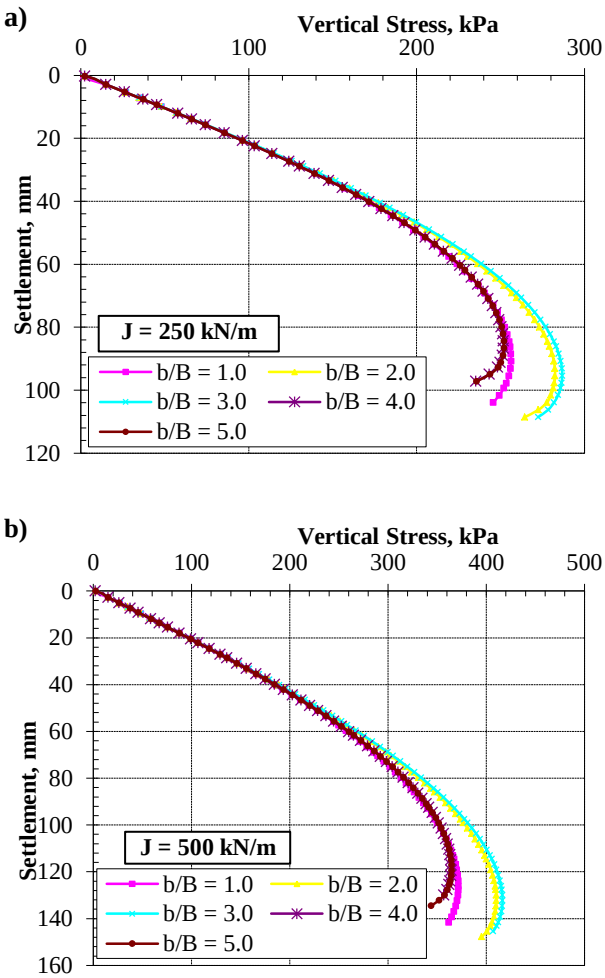

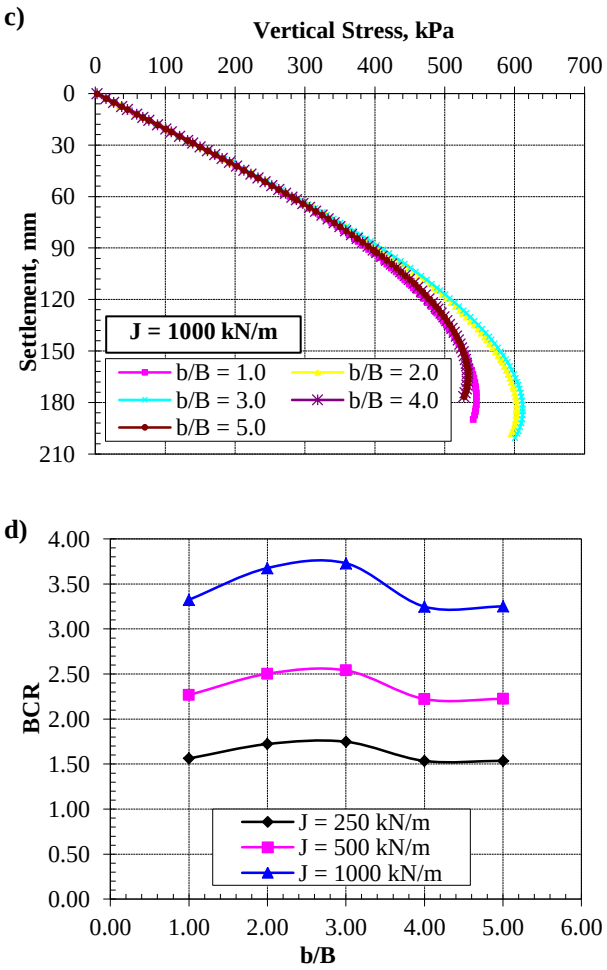

Figure 6: Settlement versus vertical stress for different values of b/B; a) J = 250 kN/m, b) J = 500 kN/m, c) J = 1000 kN/m, and d) BCR value versus (b/B) ratio.

3.2.3 Vertical Spacing between Geogrid-Layers (h/B)

Figure 7 shows the relationship between settlement and vertical stress under square footing resting on the geogrid-reinforced fine sand. The first geogrid-layer depth (u/B) is 0.30 and the geogrid-layer width (b/B) is 3.0, while the depth of subsequent geogrid-layer (h/B) changes from 0.10 to 0.40 with an increment of 0.10. The (BCR) value increases with geogrid axial stiffness and decreases with increasing (h/B) values. At a (h/B) ratio of 0.10, the (BCR) values are 2.31, 3.38 and 4.80 for the geogrid axial stiffness (J) of 250 kN/m, 500 kN/m and 1000 kN/m, respectively. When the geogrid axial stiffness (J) increases from 250 kN/m to 500 kN/m, the (BCR) value increases by 1.46 times, and when the geogrid axial stiffness increases from 250 kN/m to 1000 kN/m, it increases by 2.08 times. The results indicate the (BCR) values decrease with increasing (h/B) values; the optimal value of the (h/B) ratio is 0.15 in order to achieve a greater embedded depth of the geogrid-layer, to allow a full interlocking between it and fine sand, and to protect the geogrid-layer from environmental effects. Figure 7-b illustrates the relationship between (BCR) value and geogrid axial stiffness (J) at the optimal value of (h/B) = 0.15. In the numerical study, the values of geogrid axial stiffness are increased to 2500 kN/m in an attempt to drive a fitting equation as described in Equation (10).

$$BCR = 1.67x\ln(J) - 6.88 \qquad (h/B = 0.15) \qquad (10)$$

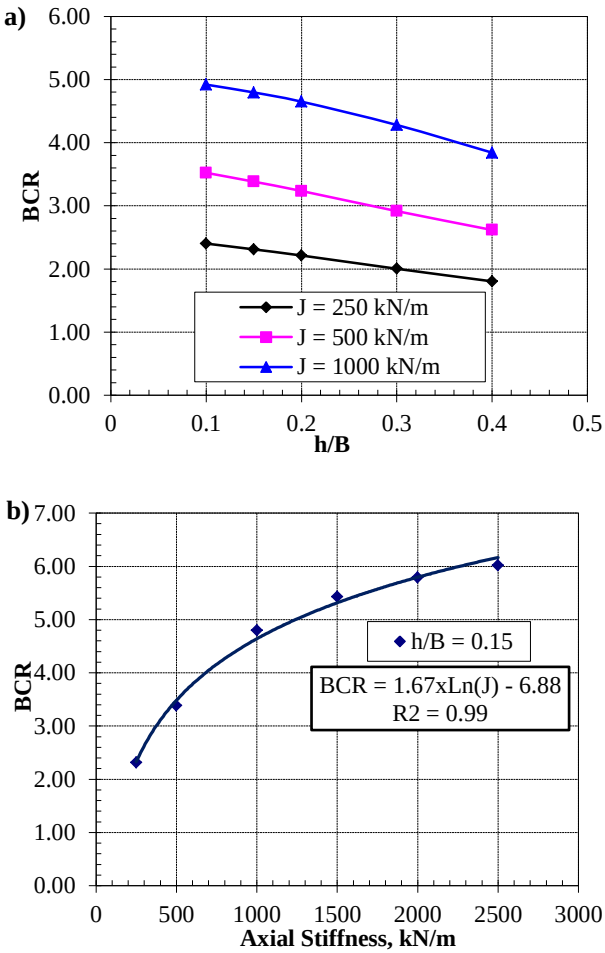

Figure 7: Vertical Spacing between Geogrid-Layers (h/B); a) BCR values versus (h/B), and b) BCR values versus geogrid axial stiffness.

3.2.4 Number of geogrid-layers (N)

The number of geogrid-layers (N) is the main affecting parameter on load-carrying capacity of geogrid-reinforced fine sand. A numerical model is conducted at the optimal values of (u/B), (b/B) and (h/B); these values are 0.30, 3.0 and 0.15, respectively. For different values of the geogrid axial stiffness of 250, 500 and 1000 kN/m, the number of geogrid-layers (N) is varied from 1.0 to 5.0 with an increment of 1.0 layer. Figure 8 shows the relationship between the bearing capacity ratio and the number of geogrid-layers when the geogrid axial stiffness is 250 kN/m, 500 kN/m and 1000 kN/m. The numerical results show the (BCR) values increase with the geogrid-layers number

until they reach N = 3.0 and remain constant thereafter. The optimal geogrid-layers number is 3.0 for a square footing that rests on geogrid-reinforced fine sand. The (BCR) values at geogrid-layers number of 3 layers are 2.50, 3.67, and 5.02 for geogrid axial stiffness of 250 kN/m, 500 kN/m, and 1000 kN/m, respectively. Figure 6-b shows an attempt to derive an equation that representing the relationship between bearing capacity ratio and the geogrid axial stiffness at the optimal value of the geogrid-layers number of (N = 3.0) described in Equation (11).

$$BCR = 1.62x\ln(J) - 6.34 \qquad (N = 3.0) \qquad (11)$$

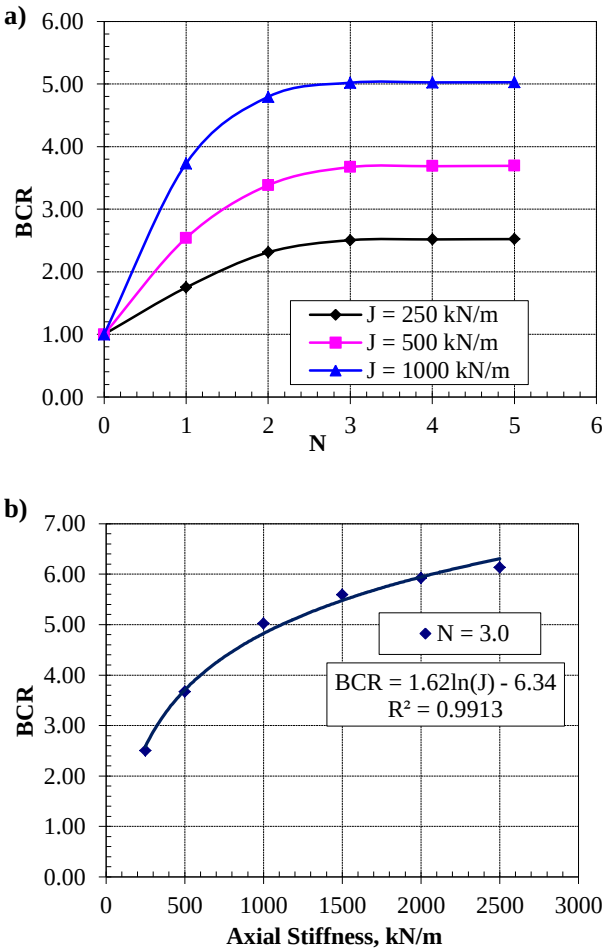

Figure 8: Number of Geogrid Layers Effect (N); a) Bearing capacity ratio (BCR) versus (N), and b) Bearing capacity ratio versus geogrid axial stiffness (J).

3.2.5 Effect of square footing size (B)

In this section, the effect of square footing size on the bearing capacity ratio of reinforced fine sand with different axial stiffness is investigated. The values of (u/B), (b/B) and the number of geogrid layers (N) are 0.30, 3.0 and 1.0, respectively. The square footing dimensions are 1.50 m x 1.50 m, 2.0 m x 2.0 m and 2.50 m x 2.50 m. The relationship between bearing capacity ratio (BCR) and geogrid axial stiffness (J) is shown in Figure 9. The results show that the (BCR) increases with geogrid axial stiffness (J) and decreases with footing sizes. Equations (12), (9) and (13) show the relationship between (BCR) and (J) for footing widths of 1.50 m, 2.0 m and 2.50 m, respectively.

$$BCR = 1.69x\ln(J) - 7.24 \qquad (B = 1.50) \qquad (12)$$
$$BCR = 1.67x\ln(J) - 7.65 \qquad (B = 2.00) \qquad (9)$$
$$BCR = 1.51x\ln(J) - 7.23 \qquad (B = 2.50) \qquad (13)$$

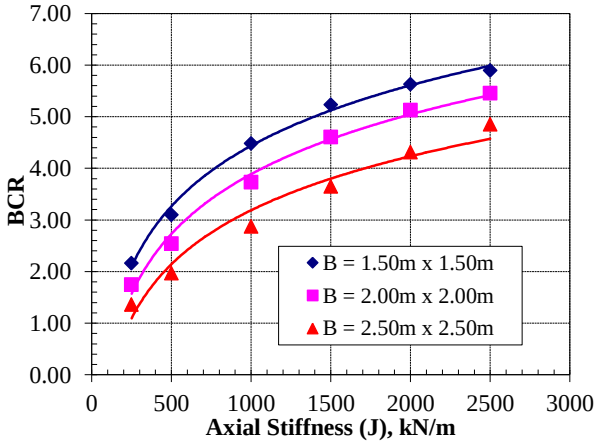

Figure 9: Bearing capacity ratio (BCR) versus geogrid axial stiffness (J) at various square footing sizes.

4. CONCLUSIONS

In this paper, a numerical analysis of the square footing on fine sand soil reinforced with a geogrid-layer with different axial stiffness is presented. The Based on the results of the current work, the following conclusions can be drawn:

- The validation of the numerical model with the experimental results of Hotti and Gupta agrees with a ratio of 98% and 93%, respectively.
- The provision of a geogrid-layer with appropriate dimensions and numbers, the bearing capacity of square footings on fine sand is significantly increased.
- The bearing capacity of reinforced fine sand increases with the geogrid axial stiffness. the increase in the bearing capacity ratio is 1.45 times and 2.13 times when the geogrid axial stiffness increases from 250 kN/m to 500 kN/m and from 250 kN/m to 1000 kN/m, respectively.
- The maximum bearing capacity ratio of the reinforced fine sand is achieved when the (u/B) ratio is 0.30 for all values of the geogrid axial stiffness.

- The optimal value of the (b/B) ratio of the geogrid-layer under the square footing is 3.0 for all values of geogrid axial stiffness.
- The optimal vertical spacing (h/B) between successive geogrid-layers is about 0.15 times the square footing width for all values of geogrid axial stiffness.
- The numerical results illustrate that the optimal geogrid-layers number is 3.0 layers for all values of geogrid axial stiffness.

STATEMENTS AND DECLARATIONS

Competing interests: The authors declare that they have no known competing financial interests or personal relationships that could have appeared to influence the work reported in this paper.

Funding: This manuscript has no funding

5. REFERENCES

[1] Braja M. Das, Shallow Foundation Bearing Capacity and Settlement, Second. New York, 2009.

[2] R. Manisana, N. N. Patil, H. M. R. Swamy, and R. Shivashankar, "Load – Settlement Characteristics of Reinforced and Unreinforced Foundation Soil," vol. 3, no. 5, pp. 888–892, 2014.

[3] M. A. Rowshanzamir and M. Karimian, "Bearing capacity of square footings on sand reinforced with dissimilar geogrid layers," Sci. Iran., vol. 23, no. 1, pp. 36–44, 2016, doi: 10.24200/sci.2016.2095.

[4] B. Hotti, P. G. Rakaraddi, and Sudharani Kodde, "Behavior of Square Footing Resting on Reinforced Sand Subjected To Incremental Loading and Unloading," Int. J. Res. Eng. Technol., vol. 3, no. 6, pp. 1–9, 2014, doi: DOI:10.15623/ijret.2014.0318011.

[5] R. Budania, R. P. Arora, B. S. Singhvi, and H. Kumar, "Performance Study of Square Footing Resting Over Geo-Grid Reinforced Sand," Int. J. Eng. Res. Appl., vol. 7, no. 2, pp. 54–59, 2017, doi: 10.9790/9622.

[6] A. Mudgal, R. Sarkar, and A. K. Shrivastava, "Bearing capacity behaviour of geosynthetics reinforced soil," Int. J. Innov. Technol. Explor. Eng., vol. 8, no. 8, pp. 2974–2979, Jun. 2019.

[7] A. Shrigondekar and P. Ullagaddi, "Bearing capacity analysis of a square footing supported on geogrid reinforced sand," Int. J. Emerg. Technol., vol. 11, no. 3, pp. 169–176, 2020.

[8] H. A. J. Hassan and R. R. Shakir, "Ultimate bearing capacity of eccentrically loaded square footing over geogrid-reinforced cohesive soil," J. Mech. Behav. Mater., vol. 31, no. 1, pp. 337–344, 2022, doi: 10.1515/jmbm-2022-0035.

[9] S. K. Das and N. K. Samadhiya, "A numerical parametric study on the efficiency of prestressed geogrid reinforced soil," in E3S Web of Conferences, EDP Sciences, Nov. 2020. doi: 10.1051/e3sconf/202020512004.

[10] R. J. Bathurst, F. M. Naftchali, and R. Jamshidi Chenari, "The role of geosynthetic stiffness in soil reinforcement applications," E3S Web Conf., vol. 368, 2023, doi: 10.1051/e3sconf/202336801002.

[11] C. A. E. User, "Abaqus theory manual," Abaqus 6.13 Doc., no. Dassault Systemes Simulia Corp., Providence, RI, USA., 2014.

[12] S. Helwany, Applied Soil Mechanics: With ABAQUS Applications. John Wiley and Sons, 2007. doi: 10.1002/9780470168097.

[13] S. S. Park and P. M. Byrne, "Stress densification and its evaluation," Can. Geotech. J., vol. 41, no. 1, pp. 181–186, 2004, doi: 10.1139/t03-076.

[14] A. J. Lutenegger and M. T. Adams, "Bearing Capacity of Footings on Compacted Sand," in 4th International Conference on Case Histories in Geotechnical Engineering, 1998, pp. 1216–1224.

[15] P. K. Kolay, S. Kumar, and D. Tiwari, "Improvement of Bearing Capacity of Shallow Foundation on Geogrid Reinforced Silty Clay and Sand," J. Constr. Eng., vol. 2013, no. Article ID 293809, pp. 1–10, 2013, doi: http://dx.doi.org/10.1155/2013/293809.

[16] A. B. Cerato and A. J. Lutenegger, "Scale effects of shallow foundation bearing capacity on granular material," J. Geotech. Geoenvironmental Eng., vol. 133, no. 10, pp. 217–225, 2007, doi: https://doi.org/10.1061/(ASCE)1090-0241(2007)133:10(1192).

[17] A. Gupta and T. G. Sitharam, "Experimental and numerical investigations on interference of closely spaced square footings on sand," Int. J. Geotech. Eng., vol. 14, no. 12, pp. 1–9, 2018, DOI:10.1080/19386362.2018.1454386.